Journal of Thermal Analysis and Calorimetry
https://doi.org/10.1007/s10973-026-15833-5

7E analysis and sustainability evaluation of dual-passage solar thermal air collector with staggered turbulators

Abhishek Thakur[1,7,8] · Sashank Thapa[2,7,8] · Tej Singh[3,7,8] · Raj Kumar[4,7,8] · Daeho Lee[4,7,8] · Hüseyin Bakır[5,7,8] · Ümit Ağbulut[6,7,8]

Received: 14 November 2025 / Accepted: 8 June 2026
© The Author(s) 2026

Abstract

The present research investigates and evaluates the performance of a dual-passage solar thermal air collector integrated with a staggered turbulator configuration using an analytical approach. Based on an analysis of energy and exergy, the impact of the staggered turbulator geometrical parameters on the dual-passage solar thermal air collector performance is evaluated analytically, and the findings have been compared with a traditional smooth plate. The current investigation analytically assesses the exergetic, effective, and thermal efficiencies of a dual-passage solar thermal air collector roughened with single V-shaped staggered baffles. A parametric design and temperature rise parameter are used to assess these efficiencies in order to accurately forecast the dual-passage solar thermal air collector energy consumption. Economic analysis, environmental analysis, enviroeconomic analysis, exergoeconomic analysis, exergoenvironmental analysis, and sustainability index are also examined by energetic and exergetic analytical research results. In accordance with the dual-passage solar thermal air collector system's economic evaluation, the energy cost is determined to be 0.077 USD kWh^{-1}. The exergoeconomic and exergoenvironmental parameters are calculated to be 0.1716 kWh USD^{-1} and 0.5305 tons of CO_2 over its life cycle. According to the enviroeconomic and environmental analysis, the dual-passage solar thermal air collector can mitigate 39.95 tons of CO_2 over its life cycle (10 years), and the amount of earned carbon credit obtained is 579.27 USD.

Keywords Dual-passage solar thermal air collector · Thermal efficiency · Effective efficiency · Exergy efficiency · Enviroeconomic · Sustainability index

Abbreviations

A_{AP}	Absorber plate area, m^2
Nu_{SP}	Nusselt number of smooth plate
B	Staggered baffle size, m
N_{gc}	Number of glass covers
B/H_{BF}	Relative staggered baffle size
Pr	Prandtl number
C_{PA}	Air specific heat, J kg^{-1} K^{-1}
P_{BF}	Roughness pattern pitch, m
D_H	Hydraulic diameter of channel, m
P'_{BF}	Staggered baffles pitch, m

✉ Raj Kumar
errajap@gmail.com

✉ Ümit Ağbulut
umit.agbulut@yildiz.edu.tr

[1] School of Physics & Materials Science, Shoolini University, Solan, H.P. 173229, India

[2] Faculty of Engineering and Technology, Shoolini University, Solan, Himachal Pradesh, India

[3] Faculty of Informatics, ELTE Eötvös Loránd University, Budapest 1117, Hungary

[4] Department of Mechanical Engineering, Gachon University, 1342, Seongnamdaero, Sujeong-Gu, Seongnam 13120, South Korea

[5] Department of Electronics and Automation, Vocational School, Dogus University, Istanbul, Türkiye

[6] Department of Mechanical Engineering, Faculty of Mechanical Engineering, Yildiz Technical University, Istanbul, Türkiye

[7] Information Technologies Research and Application Center, Istanbul Ticaret University, 34445 Istanbul, Türkiye

[8] Department of Technical Sciences, Western Caspian University, Baku, Azerbaijan

Published online: 31 July 2026

E_{SR}	Exergy flow associated with solar irradiance, W
P_{BF}/H_{BF}	Relative roughness pitch
E_F	Exergy flow of fluid, W
P'_{BF}/P_{BF}	Relative staggered baffle position
f_{BF}	Friction factor of baffled plate
Q_u	Useful energy gain rate, W
f_{SP}	Friction factor for smooth plate
DP-STAC	Dual-passage solar thermal air collector
$\ddot{F}$	Plate efficiency factor
Q_{OL}	Optical losses, W
F_{RF}	Heat removal factor
Q_{TL}	Thermal losses to the environment, W
g	Gap width, m
Re_{XX}	Reynolds number
g/H_{BF}	Relative gap size
T_{PM}	Bulk mean plate temperature, K
G_D/L_{SV}	Relative gap position
T_{FM}	Bulk mean fluid temperature (air), K
G	Mass velocity, kg s^{-1} m^{-2}
t_e	Collector edge thickness, m
RE	Renewable energy
SI	Sustainability index
H_{BF}/H_{CH}	Relative roughness height
ΔP_D	Pressure drop, Pa
h_c	Heat transfer coefficient, W m^{-2} K^{-1}
T_{IA}	Inlet mean temperature (air), K
H_{BF}	Baffle height, m
T_{OA}	Outlet mean temperature (air), K
I_{SR}	Intensity of solar radiation (W m^{-2})
T_{AB}	Ambient temperature, K
H_{CH}	Height of the channel, m
ΔT	Channel air temperature difference, K
L_{TS}	Length of test section, m
$\Delta T/I_{SR}$	Temperature rise parameter, (Km^2/W)
L_{AG}	Gap of air between glass cover and absorber plate, m
U_{LC}	Overall coefficient of heat loss, W m^{-2} K^{-1}
L_{SV}	Single V-baffles length, m
v_a	Velocity (air), m s^{-1}
m_a	Mass flow rate (air), kg s^{-1}
α_{BF}	Angle of attack (°)
Nu_{BF}	Nusselt number of baffled plate
ε_{AP}	Absorber plate emissivity
W_{CH}	Width of the channel, m
ε_{GC}	Emissivity of glass cover
W_v	Wind velocity (m s^{-1})
η_{TH}	Thermal efficiency
STAC	Solar thermal air collector
η_{EFF}	Effective efficiency
AP	Absorber plate
η_{EX}	Exergy efficiency
AR	Artificial roughness
η_{THPP}/THPP	Thermohydraulic performance parameter
HT	Heat transfer
η_{CARNOT}	Carnot efficiency
SAH	Solar air heater
$\tau\alpha_P$	Transmissivity–absorptivity product
SE	Solar energy
ρ_a	Density of air, kg m^{-3}
SVSSBs	Single V-shaped staggered baffles
k_a	Fluid thermal conductivity (air), W m^{-1} K^{-1}
STC	Solar thermal collector
k_i	Thermal conductivity of glass wool, (W m^{-1} K^{-1})
TP	Thermal performance
δ_b	Thickness of the insulation at the base, m
f	Friction factor
n	Lifetime of solar thermal air collector, 10 Years
USD	United State Dollar

Introduction

The global energy sector is facing unprecedented challenges due to increasing energy demand. Today's energy crisis affects all fossil fuel markets, with record-high natural gas and oil prices. Energy price variations cause inflation, industrial limitations, and slower economic development in many places. The multiple forms of energy are crucial in determining global economic advancement and commercialization. The global population is continually expanding, hence elevating the need for energy to meet the needs of private and industrial consumers. Both advanced and developing nations have sought to generate energy without harming the environment, particularly with CO_2 emissions. Renewable energy (RE) supplies can efficiently fulfill energy demands. RE encompasses extensive research and has the potential to substitute non-renewable energy sources in the future. Solar energy is a primary RE resource that is clean, safe, free and abundantly available [1, 2]. The straightforward and effective method of harnessing SE is to turn it into thermal energy via solar thermal collectors (STCs). These systems are simplistic in design, economically viable and adaptable for design enhancements. However, it is crucial to acknowledge that solar thermal air collectors (STACs) suffer from lower TP because of the poor thermal conductivity of air. Numerous research studies have addressed this problem by developing strategies to improve STAC performance. These strategies include the use of obstacles, differently shaped baffles, and chemical surface treatments [3, 4]. Additionally, some methods

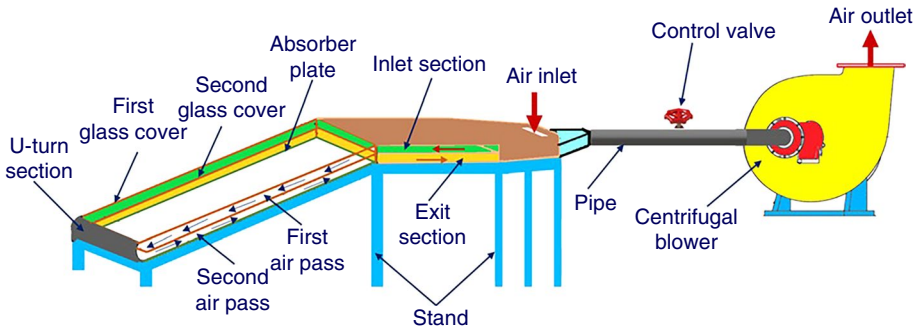

Fig. 1 Schematic representation of the testing setup

utilize finned and extended surface absorbers [5], expanded heat transfer features such as porous and corrugated surfaces [6], artificial roughness (AR) on the absorber, and impinging air jets [7]. AR induces turbulence in the flow, leading to increased fluid mixing and disrupting the formation of the thermal boundary layer, which contributes to improved heat transmission [8]. Many kinds of STAC are designed according to specific requirements. A dual-passage solar thermal air collector (DP-STAC) has higher thermal performance relative to a single-pass STAC. A variety of investigators have contributed to developing the idea of the performance enhancement of DP-STAC. Ravi and Saini [9] reviewed numerous studies on improving the performance of double-pass solar air heaters (DP-SAHs). The findings of the evaluation indicate that most of the investigation was conducted on double-pass systems with expanded surfaces and packed bed materials. Pachori et al. [10] provided a comprehensive analysis of the variety of DP-SAH approaches that are viable. El-khawajah et al. [11] examined the thermal performance (TP) of a DP-SAH with 2, 4, and 6 fins via experimentation. The finding shows that DP-SAH with 2, 4, and 6 fins achieved maximum efficiency of 75%, 82.1%, and 85.9%, respectively, at a mass flow rate of 0.042 kg s^{-1}. Abo-Elfadla et al. [12] carried out an experimental study to investigate the effect of a new design AP on the TP of an SAH at distinct mass flow rates. Baig and Ali [13] worked on multiple analyses to assess the efficacy of a DP-SAH under frigid winter settings. Sajawal et al. [14] examined the η_{TH} of DP-SAH by integrating PCM within metal tubes with fins to enhance energy storage and HT. Omojaro and Aldabbagh [15] executed a test study of the TP of single-pass and DP-SAHs with fins, employing a wire made of steel mesh as the AP. The results they reported demonstrate that at a mass flow rate of 0.038 kg s^{-1}, the peak efficiencies attained reached 59.62% for the single-pass system and 63.74% for the DP-SAH. Aldabbagh et al. [16] analyzed the η_{TH} of single-pass and DP-SAH systems utilizing wire mesh in place of traditional smooth absorbent surface. The findings demonstrate that within the examined mass flow rate which varied from 0.012 to 0.038 kg s^{-1}, efficiency rises with a increase in mass flow rate. The highest η_{TH} observed were 45.93% for the single pass and 83.65% for the DP-SAH at a mass flow rate of 0.038 kg s^{-1}. El-Sebaii et al. [17] performed both theoretical and numerical assessments of v-corrugated DP-SAH. Mathematical predictions substantially corresponded with actual performance. The research examined the influence of mass flow rate on η_{TH}, and η_{THP} of DP-SAH. The findings demonstrate that the v-corrugated DP-SAH was 11–14% more effective than the traditional DP-SAH. Raj et al. [18] examined forced convection HT in a DP-SAH intended for solar-dried agricultural products, employing an asymmetrical duct flow arrangement. Kumar et al. [19] examined the TP of DP-SAH ducts using a shot-blasted AP affixed to winglets. The findings demonstrate that the shot-blasted AP, including winglets improves η_{TH} by generating disturbance and enlarging the entire surface area used for HT. Thakur et al. [20] implemented a research study on the effect of a staggered turbulator on the η_{THPP} of a DP-STAC. Finding showed that the η_{THPP} attained its highest value of 3.67 for the arrangement featuring single V-shaped staggered baffles at P_{BF}/H_{BF} of 1.5, P'_{BF}/P_{BF} of 0.65, and B/H_{BF} of 3.5 Re_{XX}= 17,000. Assadeg et al. [21] assessed the influence of mass flow rate and I_{SR} on the energy efficiency, η_{EX}, and improved potential. At a mass flow rate = 0.15 kg sec^{-1}, the collector energy efficiency was 73%. At the highest level I_{SR}=1000 W m^{-2}, the η_{EX} is around 2.5–4.2%, at I_{SR} levels between 425 and 1000 W m^{-2}, the lowest and greatest improvement potentials are 980-2287W. Hedayatizadeh et al. [22] performed an exergetic examination of a v-corrugated DP-SAH. As a result, thorough thermal modeling of the specified DP-SAH is completed and verified by literature that demonstrates strong agreement. The best η_{EX}, of the specified v-corrugated DP-SAH was increased by 6.27% according to simulation. Abo-Elfadl et al. [23] explored the efficacy of an innovative tubular solar air heater (T-SAH) of neighboring parallel tubes, focusing on energy, exergy, and environmental analysis. The research evaluated the efficacy of T-SAH and F-SAH at varying air mass flow rates of 0.075, 0.05, and 0.025 kg s^{-1}. The projected carbon credits from the reduced CO_2 were USD 391.6 annually for F-SAH and USD 561.9 per year for T-SAH at a mass flow rate of 0.075 kg s^{-1}. Fahmi et al. [24] conducted an energy and exergy analysis

of a DP-SAH with finned plates in various configurations. To augment the DP-SAH energy and exergy efficiency, Velmurugan and Kalaivanan [25] used DP-SAH with various absorber surface geometries. Using an indoor solar simulator, the impact of varying mass flow rate and I_{SR} on air temperature increase, η_{TH}, η_{EX}, and ΔP_D under steady-state conditions was assessed across various STAC types. Machi et al. [26] assessed the effectiveness of a DP-SAC with triangular integrated fins via experimentation. Two identically designed collectors, one with fins and one without, were tested in order to assess the collector's η_{TH}. Finned collectors had daily η_{TH} of 56.57%, 59.41%, and 61.42%, while unfinned collectors had daily η_{TH} of 51.04%, 53.28%, and 57.08% at mass flow rates of 0.0081, 0.0101, and 0.0121 kg s^{-1}. The η_{TH} of the finned DP-SAC was 4.3% to 6.1% higher than that of the unfinned one.

In the field of solar energy technology, a myriad of research has been carried out with the implementation of AR in STAC. The AR increases the thermal performance with the production of turbulent and secondary flow in the main fluid flow. The thermal performance increases on account of the ΔP_D and, hence, the pumping power requirement. There is limited emphasis on the integrated approach to studying thermal performance with effective and second law efficiency, along with the environmental and sustainability outcomes. To address these research gaps, the present study, based on earlier experimental research [20], proposes a comprehensive analytical framework based on a 7E approach, encompassing energy, exergy, economic, environmental, enviroeconomic, exergoeconomic, and exergoenvironmental analyses of a DP-STAC with staggered turbulators. To the best of the authors' knowledge, no such comprehensive study for a DP-STAC with staggered turbulators has been reported, especially with the 7E approach in terms of assessment of quality energy output, sustainability and environmental analysis. This represents the key novelty of the present work.

Evaluation of DP-STAC performance

The outdoor setup of the DP-STAC system was systematically designed, constructed, and evaluated under real environmental conditions to facilitate data acquisition. The DP-STAC has two separate airflow channels: one between the upper and lower glass covers and one between the lower glass cover and the AP. The galvanized iron (G.I.) sheet is utilized as the AP. Utilizing a centrifugal blower, air is drawn via the duct system, with mass flow rate adjusted via a variac transformer. Utilizing a micro-manometer ΔP_D is measured. The T_{IA}, T_{OA}, T_{PM}, and other key points are measured using T-type thermocouples. A solar power meter records the I_{SR} at multiple locations, while airflow velocity inside the ducts is monitored with an anemometer. Figure 1 provides a schematic representation of the testing setup.

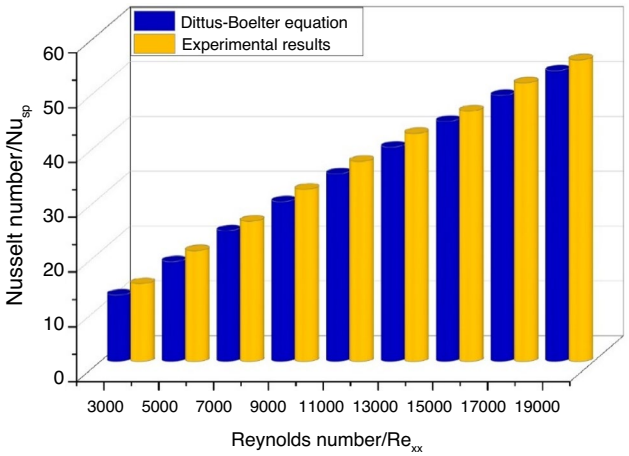

Fig. 2 Comparison of the expected and observed outcomes of Nu_{SP} [20]

The smooth duct of the testing apparatus has been validated by correlations identified in existing literature. The Nu_{SP} for the smooth plate is compared with the Dittus–Boelter equation, as delineated in Eq. (1). The f_{SP} acquired results for smooth duct are validated using the modified Blasius equation as shown in Eq. (2).

Correlation of the Nu_{SP} given by the Dittus–Boelter equation is presented in Eq. (1) [27, 45]:

$$\text{Dittus} - \text{Boelter equation} : Nu_{SP} = 0.023\, Re_{XX}^{0.8} Pr^{0.4} \quad (1)$$

Correlation of the f_{SP} provided by the modified Blasius equation is presented in Eq. (2) [28, 45]:

$$\text{Modified Blasius equation} : f_{SP} = 0.085\, Re_{XX}^{-0.25} \quad (2)$$

The anticipated and obtained experimental values of Nu_{SP} and f_{SP} for a smooth plate are shown in Fig. 2 and Fig. 3, respectively. The presented data exhibit substantial agreement between the computed values obtained from experimental outcomes and the anticipated values.

To improve TP, the DP-STAC has turbulators of the SVSSBs type mounted on the AP. Figure 4 shows the AP with staggered turbulators, presented in photographic and schematic views. The investigation examined the impact of distinct geometric configurations, including P'_{BF}/P_{BF}, B/H_{BF}, and P_{BF}/H_{BF}. The parameters were varied in the range from $P'_{BF}/P_{BF} = 0.45$–0.75, $B/H_{BF} = 2.5$–4.0, and $P_{BF}/H_{BF} = 1.0$–2.5 and other parameters such G_D/L_{SV}, H_{BF}/H_{CH}, g/H_{BF} and α_{BF} were fixed. During experimentation it was observed that the maximum η_{THPP}=3.67 was achieved when $P'_{BF}/P_{BF} = 0.65$, $B/H_{BF} = 3.5$, and $P_{BF}/H_{BF} = 1.5$ [20].

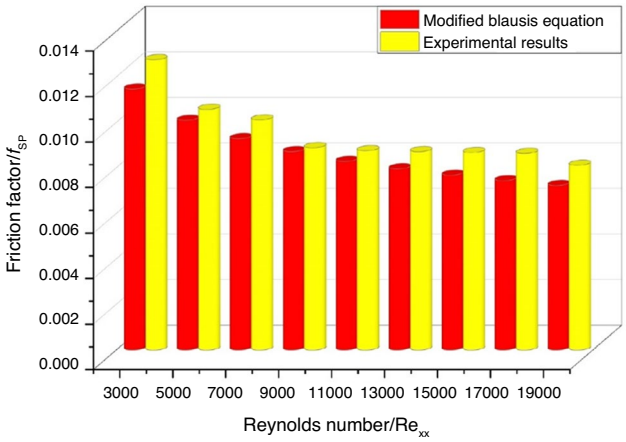

Fig. 3 Comparison of the expected and observed outcomes of f_{SP} [20]

The present study introduces an analytical approach that examines η_{TH}, η_{EFF} and η_{EX} in a DP-STAC including staggered turbulators on its AP, incorporated results from prior experimental research related to HT and its correlation development [20]. Results of energetic and exergetic analytical research include an examination of economic, environmental, enviroeconomic, exergoeconomic, exergoenvironmental and sustainability analyses.

Methodology

As previously mentioned, past investigations have focused on improving the TP of STCs using analytical and experimental methods and reporting the results in the context of energetic, exergetic, and environmental analyses. However, there has been no thorough exploration of sustainability and critical examination of 7E of a DP-STAC with staggered turbulators, specifically engineered for outdoor applications. The present research focuses on addressing this gap.

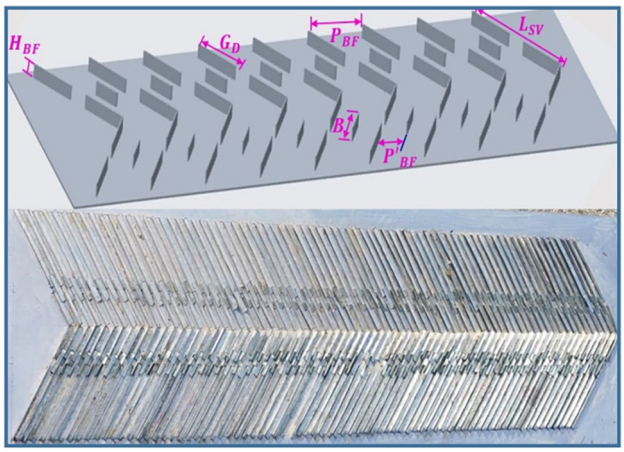

Fig. 4 Schematic and pictorial representation of the AP with staggered turbulator

Energetic and exergetic analysis

The current investigation proposes an analytical framework that analyses η_{TH}, η_{EFF} and η_{EX} in a DP-STAC with staggered turbulators on its AP, based on findings from previous experimental research based on HT and correlative development [20]. By producing turbulence and reducing ΔP_D, the optimal positioning of SVSSBs on the AP maximizes efficiency and optimizes AP design. A method of iteration is utilized to access the energy and exergetic optimization of the DP-STAC for this specific kind of roughness. The objective of this method is to reduce f_{BF} while simultaneously increasing the rate of HT. In order to maximize HT benefits and minimize pumping losses, this method challenges conventional designs by introducing a novel roughness geometry through the use of exergy analysis. The study analytically investigates the influence of turbulators design variables on the η_{TH}, η_{EFF} and η_{EX} of the DP-STAC. This thorough analysis diminishes reliance on extensive experimentation and rationalizes the assessment of design performance.

Environmental and economic analysis

According to the findings of energetic and exergetic analytical research, the economic analysis, environmental analysis, enviroeconomic analysis, exergoeconomic analysis, and exergo environmental analysis are examined**.** This comprehensive approach assesses the system's overall sustainability and efficiency. This analysis offers a thorough evaluation of the DP-STAC system's sustainability and efficiency in harnessing RE resources, hence improving its long-term profitability.

Sustainability assessment

The sustainability assessment used the SI methodology to evaluate system sustainability, emphasizing optimal resource utilization and η_{EX} [29, 30]. The SI is essential for evaluating the effectiveness of energy systems like the DP-STAC, facilitating a thorough review of economic and environmental effects. These indicators facilitate the identification of unsustainable conditions and offer guidance for system optimization. This study evaluates sustainability using η_{EX} of the DP-STAC. Assessing the SI enables a thorough analysis of DP-STAC sustainability performance, facilitating the computation of possible improvement rates and informing future design modifications to attain elevated sustainability standards.

Performance model for DP-STAC

Energetic efficiency (thermal and effective efficiency)

The Q_u of air in a DP-STAC can be expressed as proposed by [31].

$$Q_u = A_{AP}\left[I_{SR}\left(\tau\alpha_P\right) - U_{LC}\left(T_{PM} - T_{AB}\right)\right] \tag{3}$$

The useful heat gain associated with T_{IA} and T_{AB} is defined as follows [31]:

$$Q_u = A_{AP}F_{RF}[I_{SR}\left(\tau\alpha_p\right) - U_{LC}\left(T_{IA} - T_{AB}\right)] \tag{4}$$

Nevertheless, as the DP-STAC system operates on an open cycle, air temperature at T_{IA} coincides with T_{AB}. Therefore, Q_u is represented by Eq. (5).

$$Q_u = A_{AP}F_{RF}I_{SR}\left(\tau\alpha_p\right) \tag{5}$$

For an open cycle, Q_u is defined as follows [32]:

$$Q_u = F_{RF}A_{AP}[I_{SR}\left(\tau\alpha_p\right) - U_{LC}\left(T_{OA} - T_{IA}\right)] \tag{6}$$

The formula for the calculation of η_{TH} is given in Eq. (7) [31].

$$\eta_{TH} = Q_u/I_{SR}A_{AP} \tag{7}$$

Also, in terms of F_{RF}, the η_{TH} is reported by [31]:

$$\eta_{TH} = F_{RF}\left[\left(\tau\alpha_p\right) - U_{LC}\left(\frac{T_{OA} - T_{IA}}{I_{SR}}\right)\right] \tag{8}$$

The relationship between the $\ddot{F}$ and the F_{RF} is as follows [31]:

$$F_{RF} = \frac{m_aC_{PA}}{A_{AP}U_{LC}}\left[\exp\left(\frac{\ddot{F}U_{LC}A_{AP}}{m_aC_{PA}} - 1\right)\right] \tag{9}$$

The Q_u is defined by the increase in air enthalpy [31]:

$$Q_u = m_aC_{PA}(T_{OA} - T_{IA}) \tag{10}$$

It is important to recognize that the η_{TH} does not inherently account for the pumping power required to drive fluid through the passages. Therefore, to comprehensively assess the TP of the STAC, the η_{EFF} must be measured, as it incorporates both the Q_u and the frictional losses related with air flow. The expression for η_{EFF} is given as [33]:

$$\eta_{EFF} = \frac{Q_u - \left(\frac{P_f}{C_f}\right)}{I_{SR}A_{AP}} \tag{11}$$

C_f is conversion factor and represented by $C_f = \eta_f\eta_{motor}\eta_{trans}\eta_{pump}$. Here, $\eta_f = 0.65$, $\eta_{motor} = 0.88$,$\eta_{trans} = 0.925$, and $\eta_{pump} = 0.344$.

$$P_f = m_a(\Delta P_D)/\rho_a \tag{12}$$

where ΔP_D is calculated by following formula [31]:

$$\Delta P_D = \frac{4fL_{TS}\rho_aV_a{}^2}{2D_H} \tag{13}$$

Exergetic efficiency

Exergy analysis helps identify how much of the energy in moving air can actually be used by evaluating the quality-not just the quantity-of different energy inputs in a solar energy system. This includes sunlight, heat gained, losses due to friction, and other inefficiencies [34]. The useful energy transferred to the air reflects the effective heat it gains [35]. The η_{EX} is commonly described as the ratio between the useful exergy carried by the air flowing in the passage and the exergy of the I_{SR} that hits the absorber surface.

$$\eta_{EX} = \frac{E_F}{E_{SR}} \tag{14}$$

E_F and E_{SR} expressed by Eqs. (15) and (16), respectively [35].

$$E_F = I_{SR}A_{AP}\eta_{TH}\eta_{CARNOT} - P_f\left(1 - \eta_{CARNOT}\right) \tag{15}$$

$$E_{SR} = A_{AP}I_{SR}\left(1 - \frac{T_{AB}}{T_{sun}}\right) \tag{16}$$

In Eq. (15), the term η_{CARNOT} is expressed as follows:

$$\eta_{CARNOT} = \left(1 - \frac{T_{AB}}{T_{FM}}\right) \tag{17}$$

In Eq. (14), increasing E_F while keeping the denominator (E_{SR}) fixed results in a rise in η_{EX}. Consequently, energy losses must be reduced. The various elements causing exergy loss include optical, irradiation, convection, radiation and fluid losses, as detailed in the following equations [35].

$$E_{LO} = I_{SR}A_{AP}\eta_{EXE}(1 - \tau\alpha_p) \tag{18}$$

$$E_{LA} = I_{SR}A_{AP}(\tau\alpha_p)\left(\eta_{EXE} - \left(1 - \frac{T_{AB}}{T_{PM}}\right)\right) \tag{19}$$

$$E_{LE} = U_{LC}A_{AP}\left(T_{PM} - T_{AB}\right)\left(1 - \frac{T_{AB}}{T_{PM}}\right) \tag{20}$$

Table 1 Description of formulas utilized to conduct the 7E analysis and sustainability index

Analysis type	Item	Formula
Economic	Capital recovery factor (CRF) [36, 37]	$CRF = \frac{[i(1+i)^n]}{(1+i)^n-1}$
	First year annual cost (FYC) [36, 37]	$FYC = CRF \times P$ (P denotes initial cost)
	Yearly salvage value (YSV) [36]	YSV = Salvage value (SV) × Sinking fund factor (SFF) $SFF = \frac{i}{(1+i)^n-1}$
	Yearly maintenance cost (YMC) [36]	$YMC = (0.5 \times FYC)$+ (Electricity cost × CRF)
	Yearly cost (YC) [36]	$YC = YMC + FYC - YSV$
	Annual useful energy (En_{out}) [37]	En_{out}= The average of I_{SR} on the absorber surface (W/m^{-2}) $\times A_{AP}$ (m^2) × efficiency × $SD_{approx.} \times h_w$ ($SD_{approx.}$ denotes sunny days in year (approx.) and h_w is working hours/day)
	Cost of the useful energy [39]	YC/En_{out}
Environmental	Yearly reduction in CO_2 emissions [37, 42]	$\phi_{CO_2} = \frac{(En_{out} \times n) \times 2}{1000}$
Enviroeconomic	Enviroeconomic parameter (Z_{CO_2}) [37, 42]	$Z_{CO_2} = z_{CO_2} \times \phi_{CO_2}$
Exergoeconomic	Exergoeconomic parameter ($R_{g,ex}$) [36, 37]	$R_{g,ex} = \frac{Ex_{out}}{YC}$($Ex_{out}$ denotes exergy outlet)
Exergoenvironmental	Exergoenvironmental parameter [40]	$\phi_{ex,CO_2} = \frac{(Ex_{out} \times n) \times 2}{1000}$
Energy	Energy payback time [37, 38]	$(EPBT)_{en} = \frac{E_{in}}{En_{out}}$ (E_{in} denotes embodied energy)
Exergy	Exergy payback time [37, 38]	$(EPBT)_{ex} = \frac{E_{in}}{Ex_{out}}$
SI	Sustainability index [29, 30, 41, 42]	$SI = \frac{1}{1-\eta_{EX}}$

$$E_{L\Delta T} = I_{SR} A_{AP} \eta_{TH} \left(\frac{T_{AB}}{T_{FM}} - \frac{T_{AB}}{T_{PM}} \right) \quad (21)$$

Exergy losses through friction:

$$E_{L\Delta P} = m_a P_D \frac{T_{AB}}{(\rho_a T_{FM})} \quad (22)$$

Table 2 System parameter (SP) and operating parameters (OP)

Description	Parameters	Value	Parameters	Value
SP	L_{TS}(m)	1.2	t_e(m)	0.0945
	W_{CH}(m)	0.3	N_{gc}(-)	2
	H_{CH}(m)	0.025	P'_{BF}/P_{BF}	0.45–0.75
	L_{CH}(m)	2.0	B/H_{BF}	2.5–4.0
	k_i(W m^{-1} K^{-1})	0.024	P_{BF}/H_{BF}	1.0–2.5
	δ_b(m)	0.01	G_D/L_{SV}	0.67
	$\tau\alpha_P$(-)	0.81	H_{BF}/H_{CH}	0.40
	ε_{AP}(-)	0.9	g/H_{BF}	1
	ε_{GC}(-)	0.88	α_{BF}(°)	60°
	L_{AG}(m)	0.025		
OP	T_{AB}(K)	296.25	I_{SR}(W m^{-2})	1000
	T_{IA}(K)	296.25	$\Delta T/I_{SR}$ ($Km^2\ W^1$)	0.002–0.037
	W_v(m sec^{-1})	1	Re_{XX}(-)	1,800–48,000

Using collector setup, system characteristics, and operating conditions, numerical calculations are performed to assess the energy and η_{EX} at varying mass flow rates. In this work, the plate temperatures above the fluid temperature are first selected to identify different heat

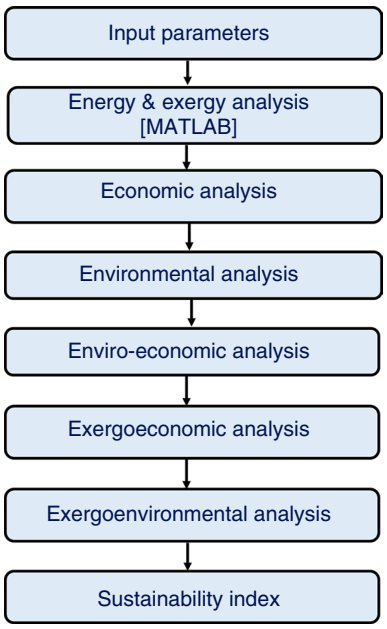

Fig. 5 Methodological procedure and computational flowchart of the comprehensive analysis

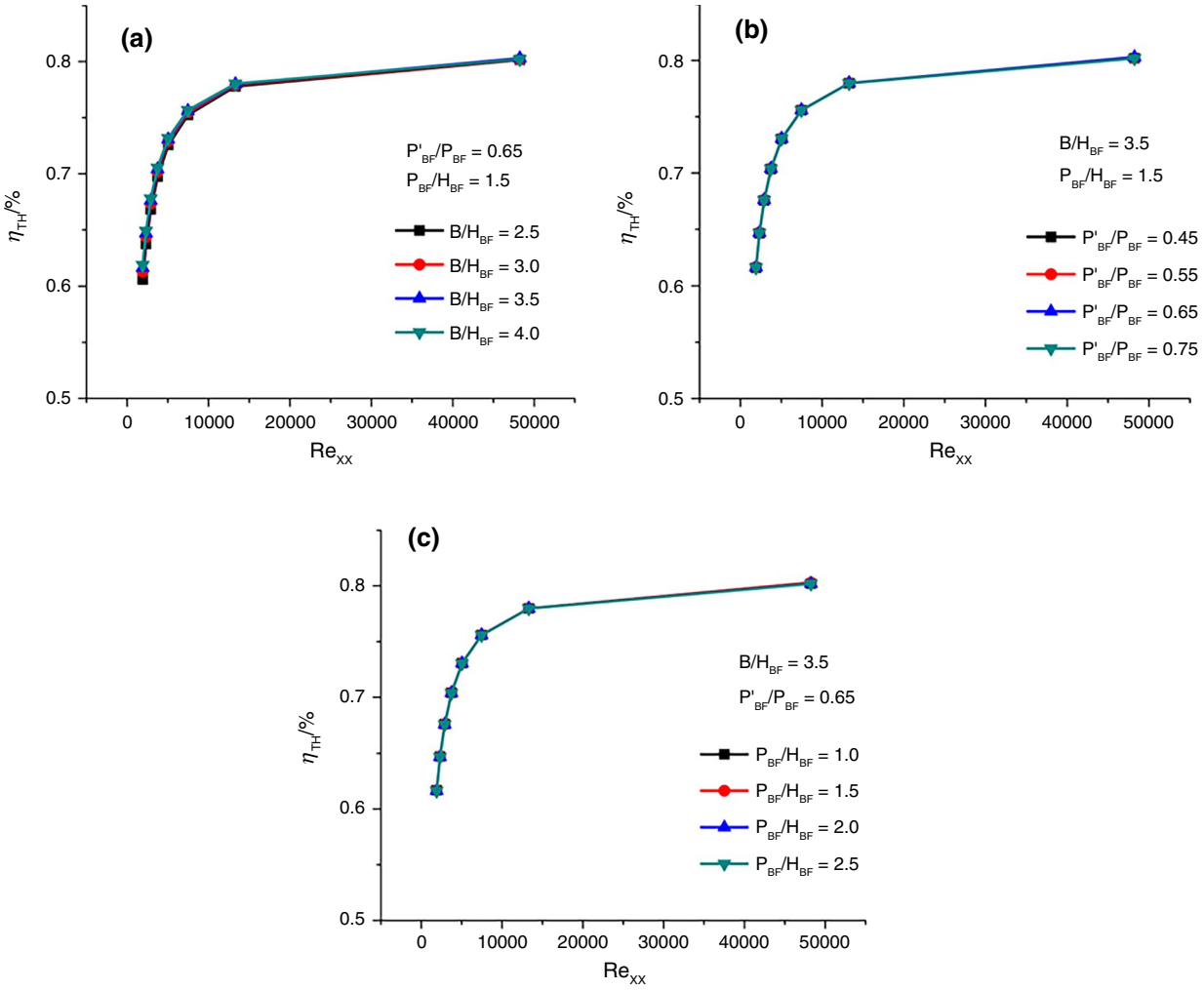

Fig. 6 Variation of η_{TH} with Re_{XX} for **a** B/H_{BF} **b** $P_{BF}^{'}/P_{BF}$ **c** P_{BF}/H_{BF}

transfer coefficients for all of the defined parameters. The Gauss–Seidel iteration method is used to determine the new temperatures (T_{NEW}) of the distinct components. The procedure will continue unless the optimum T_{NEW}) is attained within a $\pm 0.01\%$ deviation from the corresponding input values. If the T_{NEW}) are greater than 0.01% from their first values, they will be utilized as the supposed temperatures for the subsequent iteration. Codes are created in MATLAB to obtain various efficiencies analytically. The complete steps to be followed for the calculation and optimization of efficiencies with respect to geometric parameters with an extensive description provided in the Supplementary Document.

Environmental and economic analysis

The economic and environmental assessments are essential for determining the overall viability and sustainability of energy systems such as the DP-STAC. Economic, environmental, enviroeconomic, exergoeconomic, exergoenvironmental analysis and sustainability examination of proposed DP-STAC is investigated. Table 1 lists all the mathematical formulas used to carry out these analyses.

The analytical approach employed for evaluating efficiencies involves the generation of an analytical model to measure the η_{TH}, η_{EFF}, and η_{EX} across various operational and turbulator parameters, as outlined in Table 2. The flowchart presented in Fig. 5 outlines the comprehensive methodological framework adopted for the analysis.

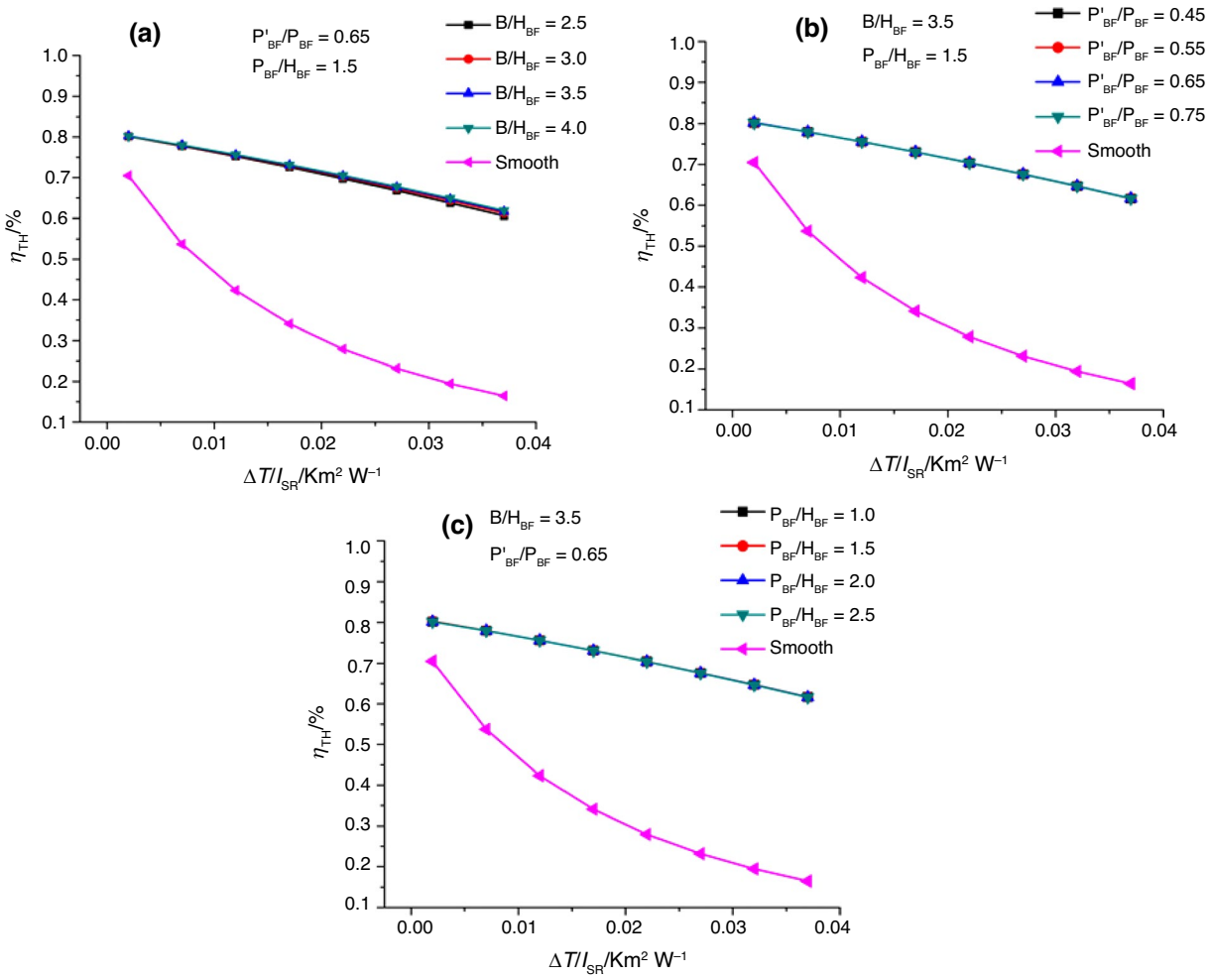

Fig. 7 Variation of η_{TH} with $\Delta T/I_{SR}$ for **a** B/H_{BF} **b** $P_{BF}^{'}/P_{BF}$ **c** P_{BF}/H_{BF}

Result and discussion

Thermal efficiency

Thermal efficiency denoted as η_{TH} representing the conversion of incoming I_{SR} into useful heat energy. It is crucial to evaluate the η_{TH} of DP-STAC, incorporating staggered turbulators. The plot of η_{TH} variations for various Re_{XX} values, alongside changes in B/H_{BF}, $P_{BF}^{'}/P_{BF}$, and P_{BF}/H_{BF} is demonstrated in Fig. 6 (a-c). The analysis presented in Fig. 6 (a-c) indicates that the η_{TH} of roughened DP-STAC was significantly improved with a rise in Re_{XX} for all roughness parameters. The higher performance of roughened DP-STAC is attributed to improved heat transfer from the baffled surface design, which augments air turbulence. The optimum roughness parameter was found to be $B/H_{BF} = 3.5$, $P_{BF}^{'}/P_{BF} = 0.65$, and $P_{BF}/H_{BF} = 1.5$ at $Re_{XX} = 48{,}000$ having η_{TH} of 80.2%.

The graph depicting η_{TH} for various $\Delta T/I_{SR}$ values, alongside changes inB/H_{BF}, $P_{BF}^{'}/P_{BF}$, andP_{BF}/H_{BF}, according to Fig. 7 (a-c). As the $\Delta T/I_{SR}$ raised, it was observed that η_{TH} significantly dropped across all parameters. The temperature difference between the base plate and the air stream diminishes when the entering fluid's temperature increases. This leads to an rise in the base plate's average temperature, resulting in increased heat dissipation to the environment and reduced beneficial heat acquisition. The η_{TH} of 80.2% is seen at$B/H_{BF} = 3.5$, $P_{BF}^{'}/P_{BF}$=0.65, and $P_{BF}/H_{BF} = 1.5$ with $\Delta T/I_{SR} = 0.002$ Km^2 W^{-1}.

Effective efficiency

The effectiveness of an STAC can be expressed as "η_{EFF}" which accounts for the advantageous energy gain alongside the necessary heat required to deliver equivalent mechanical energy to compensate pressure losses, as stated by [30].

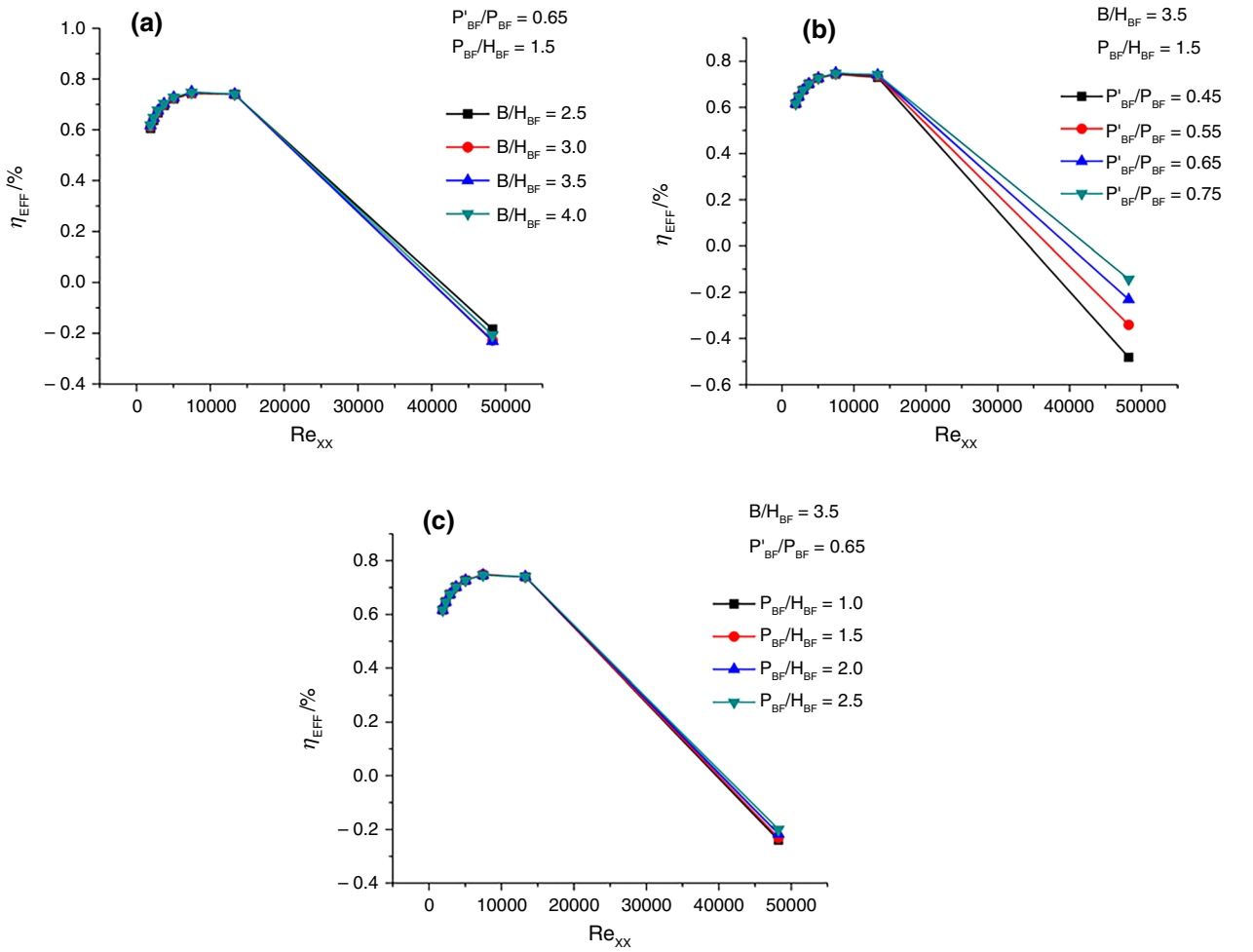

Fig. 8 Variation of η_{EFF} with Re_{XX} for **a** B/H_{BF} **b** $P^{'}_{\mathrm{BF}}/P_{\mathrm{BF}}$ **c** P_{BF}/H_{BF}

Analytical investigation was performed to find the effects of roughness variables on η_{EFF} in DP-STAC. The η_{EFF} plot variation for different Re_{XX} values, alongside changes in B/H_{BF}, $P^{'}_{\mathrm{BF}}/P_{\mathrm{BF}}$, and $P_{\mathrm{BF}}/H_{\mathrm{BF}}$ is illustrated in Fig. 8 (a-c).

Figure 8 (a) demonstrates that η_{EFF} rises with Re_{XX} for all values of B/H_{BF} and optimal efficiency is achieved at $Re_{\mathrm{XX}} = 5{,}000$–$13{,}000$ for all B/H_{BF} before frictional losses exceed the benefits of heat transfer. Similarly, from Fig. 8 (b), it can be observed that the peak η_{EFF} has become constant at a value near 74% from Re_{XX} =7,400–7,500 from and above $P^{'}_{\mathrm{BF}}/P_{\mathrm{BF}}$= 0.55 and $B/H_{\mathrm{BF}} = 3$. The optimum parameter was observed to be $B/H_{\mathrm{BF}} = 3.5$, $P^{'}_{\mathrm{BF}}/P_{\mathrm{BF}}$=0.65, and $P_{\mathrm{BF}}/H_{\mathrm{BF}} = 1.5$ which is also having maximum THPP and $\eta_{\mathrm{EFF}} = 74.6\%$. The plot of η_{EFF} variation for distinct values $\Delta T/I_{\mathrm{SR}}$ with variation in B/H_{BF}, $P^{'}_{\mathrm{BF}}/P_{\mathrm{BF}}$ and $P_{\mathrm{BF}}/H_{\mathrm{BF}}$ is as shown in Fig. 9 (a–c). The η_{EFF} noted to enhance with rising temperature, reaches the highest value, and thereafter diminishes across all parameters. Smooth DP-STAC exceeds roughened DP-STAC for $\Delta T/I_{\mathrm{SR}}$ below 0.005 $\mathrm{Km^2/W^{-1}}$, as illustrated in Fig. 9(a–c).

Exergetic efficiency

For determining the optimum values of operational and geometric parameters, η_{EX} was introduced by Altfeld et al. [35]. This investigation examines the influence of Re_{XX} onη_{EX}, utilizing MATLAB-developed software. The results indicate that η_{EX} has a positive association with Re_{XX} for a particular B/H_{BF} values, attaining a maximum value before subsequently decreasing as Re_{XX} increases, as demonstrated in Fig. 10 (a). The η_{EX} rises with an increase in B/H_{BF} from 2.5 to 3.5, after that it is constant and their no further rise in it. An $B/H_{\mathrm{BF}} = 3.5$ corresponds to a maximum η_{EX} of 1.37%. It is evident that both Nu_{BF} and f_{BF} increase when the value of B/H_{BF} rises. The staggered baffle causes the airflow to separate from both sides and the top. Furthermore, due

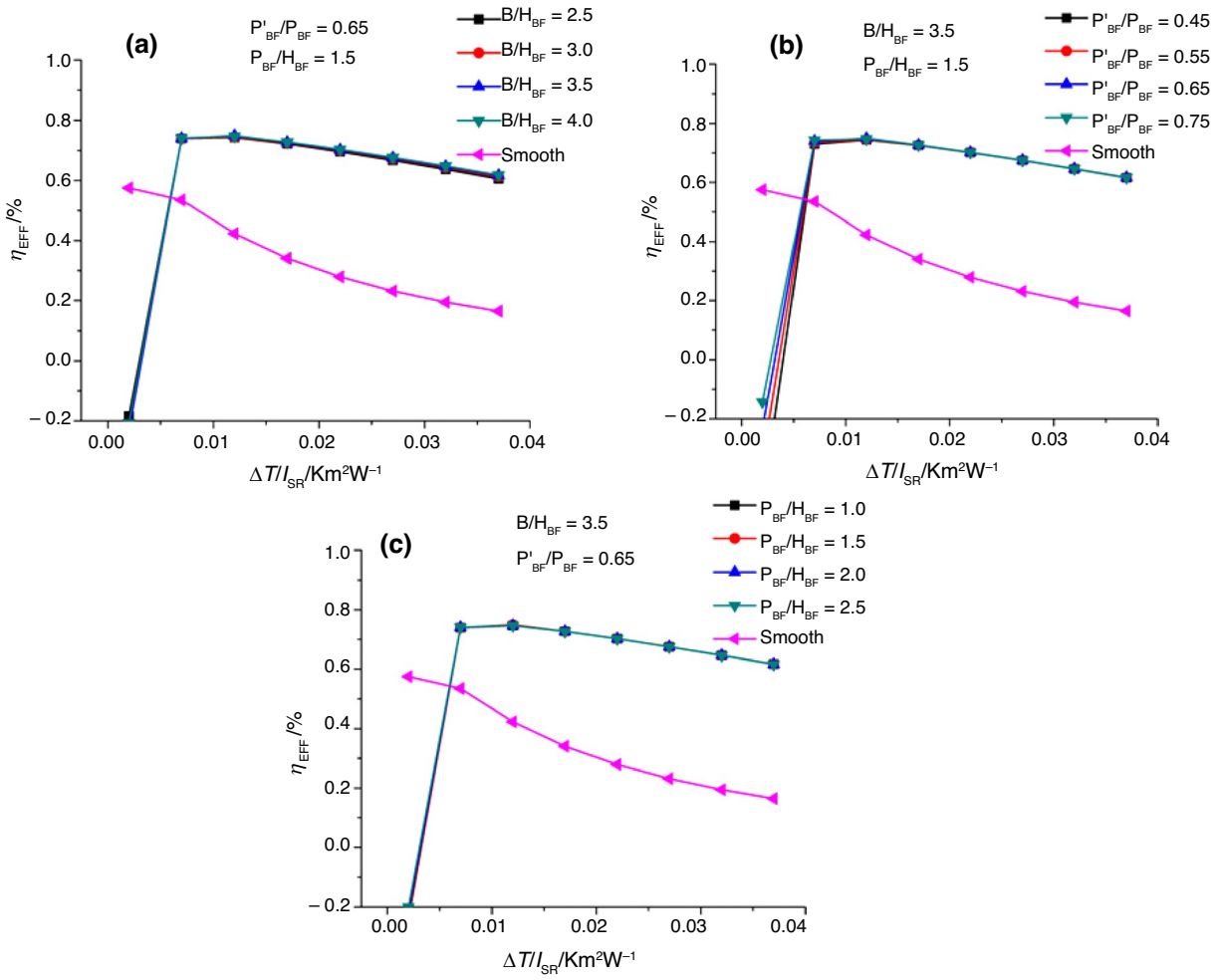

Fig. 9 Variation of η_{EFF} with $\Delta T/I_{\mathrm{SR}}$ for **a** B/H_{BF} **b** $P_{\mathrm{BF}}^{'}/P_{\mathrm{BF}}$ **c** $P_{\mathrm{BF}}/H_{\mathrm{BF}}$

to the excessive increase in f_{BF} relative toNu_{BF}, roughness geometries with B/H_{BF} values exceeding 3.5 may lead to a decrease in the thermal performance. Figure 10 (b) shows the consequence of $P_{\mathrm{BF}}^{'}/P_{\mathrm{BF}}$ onη_{EX}. The η_{EX} rises with $P_{\mathrm{BF}}^{'}/P_{\mathrm{BF}}$ from 0.45 to 0.75 with rise in Re_{XX}. The persistent rise in Nu_{BF} and f_{BF} occurs within the range of $P_{\mathrm{BF}}^{'}/P_{\mathrm{BF}} =$ 0.45 to $P_{\mathrm{BF}}^{'}/P_{\mathrm{BF}} = 0.65$. At point $P_{\mathrm{BF}}^{'}/P_{\mathrm{BF}} = 0.75$, resulting in a decrease in the Nu_{BF} value. This is due to the restriction in airflow caused by the gap for small $P_{\mathrm{BF}}^{'}/P_{\mathrm{BF}}$ values up to 0.45. Within the range of$P_{\mathrm{BF}}^{'}/P_{\mathrm{BF}}$, where $P_{\mathrm{BF}}^{'}/P_{\mathrm{BF}} = 0.45$ to $P_{\mathrm{BF}}^{'}/P_{\mathrm{BF}} = 0.65$, the airflow mixture created from the spaces with the main stream is improved, thus minimizing disruptions in the wake area caused by two consecutive baffles.

The Nu_{BF} attains its maximum value at $P_{\mathrm{BF}}^{'}/P_{\mathrm{BF}}$ equals 0.65. This happens as the flow may more efficiently rejoins because of suitable merging of flow through spaces with the main stream. This mixing is particularly effective in avoiding the redevelopment of the boundary layer. When the baffle component is situated at the position $P_{\mathrm{BF}}^{'}/P_{\mathrm{BF}} = 0.75$, it gets closer a downstream baffle, so restricting the flow entering the gaps and resulting in a diminished augmentation of HT. The effect of $P_{\mathrm{BF}}/H_{\mathrm{BF}}$ is shown in Fig. 10 (c). The η_{EX} decreases with $P_{\mathrm{BF}}/H_{\mathrm{BF}}$ from 1.0 to 2.5 with increase in Re_{XX}. It has been established that for anyRe_{XX}, the Nu_{BF} decreases as the ratio $P_{\mathrm{BF}}/H_{\mathrm{BF}}$ grows, the change in the value of Nu_{BF} is due to the stream reconnecting happening downstream of the baffle, accompanied by the reestablishment of a boundary layer up to its subsequent baffle. The distance from the reconnecting point to the upstream baffle continues to be mostly unchanged as the $P_{\mathrm{BF}}/H_{\mathrm{BF}}$ ratio grows. Nevertheless, the gap from the reconnection point to the subsequent downstream baffles rises. The inter-baffle local HT coefficient diminishes in the flow direction after reaching its maximum at the reconnection point. The optimum parameter was observed to be$B/H_{\mathrm{BF}} = 3.5$, $P_{\mathrm{BF}}^{'}/P_{\mathrm{BF}}$ =0.65, and $P_{\mathrm{BF}}/H_{\mathrm{BF}} = 1.5$ which is also having maximum THPP and$\eta_{EX} = 1.37\%$.

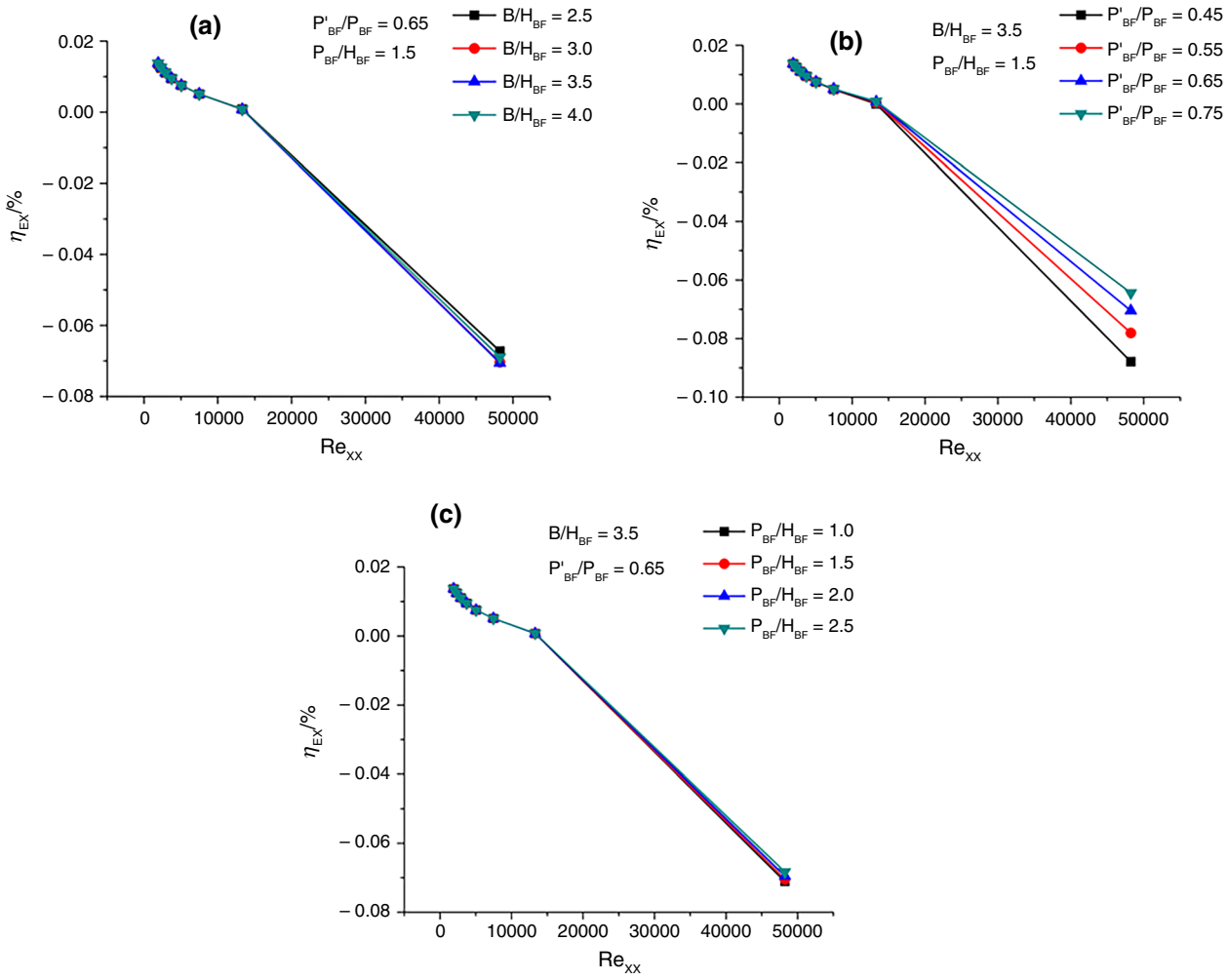

Fig. 10 Variation of η_{EX} with Re_{XX} for **a** B/H_{BF} **b** $P_{BF}^{'}/P_{BF}$ **c** P_{BF}/H_{BF}

The graph depicting the fluctuation of η_{EX} for various values of$\Delta T/I_{SR}$, alongside changes inB/H_{BF}, $P_{BF}^{'}/P_{BF}$, andP_{BF}/H_{BF}, is illustrated in Fig. 11 (a–c). The smooth plate DP-STAC demonstrates superior performance compared to the roughened DP-STAC for $\Delta T/I_{SR}$ values under 0.01 Km^2/W^{-1} across all three parameters. The smooth plate DP-STAC outperforms the roughened DP-STAC for $\Delta T/I_{SR}$ values under 0.01 $Km^2\ W^{-1}$ across all three parameters. The optimal η_{EX} is attained when$B/H_{BF} = 3.5$, $P_{BF}^{'}/P_{BF}$=0.65, and $P_{BF}/H_{BF} = 1.5$ of 0.0137 for $\Delta T/I_{SR}$ of 0.037 $Km^2\ W^{-1}$.

Economic and environmental analysis

In accordance with the SI of a DP-STAC with staggered turbulators and the examination of 7E, the energy cost of the DP-STAC is determined to be 0.077 USD kWh^{-1}. The exergoeconomic and exergoenvironmental parameter is calculated to be 0.1716 kWh USD^{-1} and 0.5305 tons of CO_2 over its life cycle. According to the environmental and enviroeconomic analysis, the DP-STAC can mitigate 39.95 tons of CO_2 over its life cycle (10 Years), and the amount of earned carbon credits is found to be 579.27 USD. The outcomes revealed that the energy payback time depends on energy and exergy is calculated to be 0.31 year and 24.07 years, respectively.

Sustainability index (SI)

Sustainability index is one of the most significant metrics that has to be taken into consideration when assessing renewable energy systems. The DP-STAC integrated with a staggered turbulator has been found to have an SI value of 1.0138, according to findings by the study results.

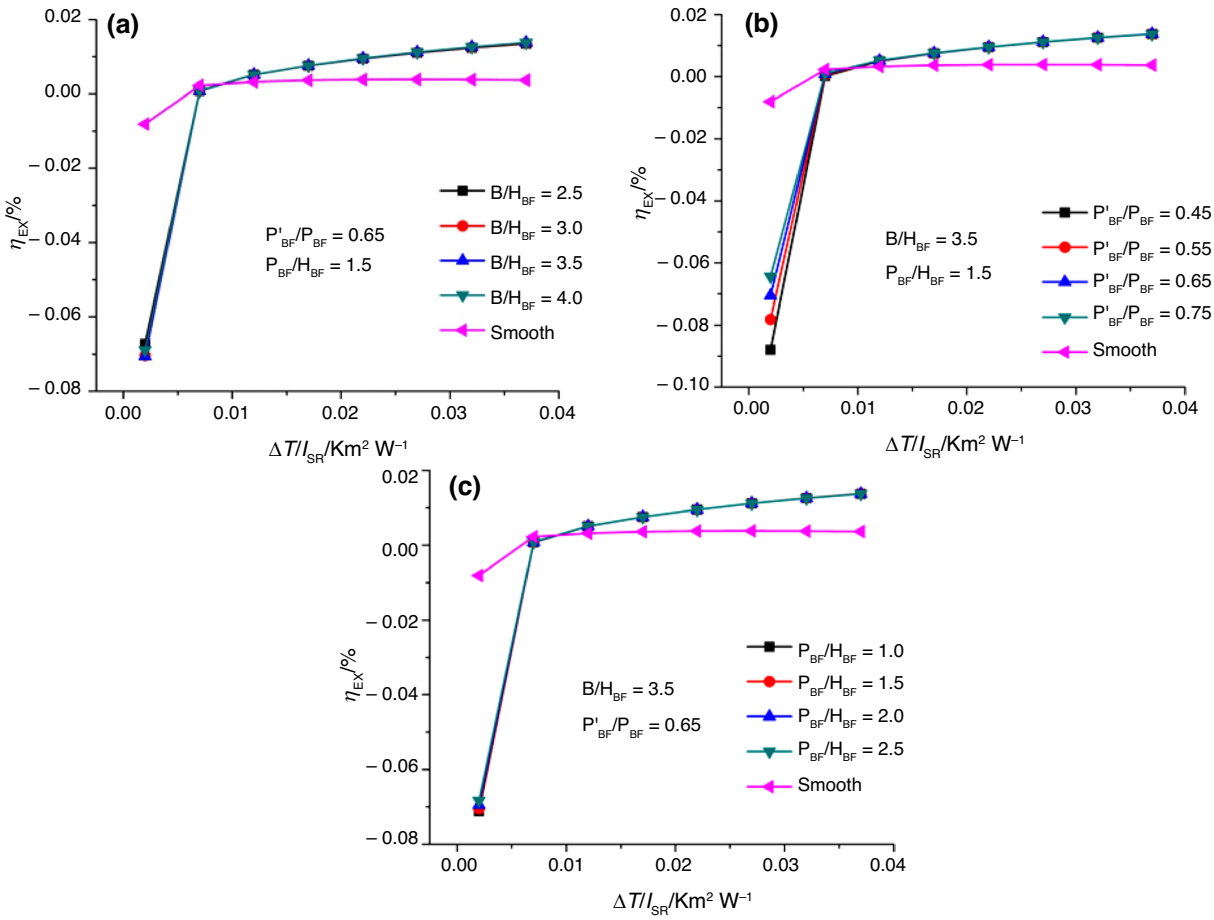

Fig. 11 Variation of η_{EX} with $\Delta T/I_{SR}$ for **a** B/H_{BF} **b** P'_{BF}/P_{BF} **c** P_{BF}/H_{BF}

Table 3 Summary of the results

Energy efficiency		η_{EX}	Economic analysis	Environmental analysis	Enviro-economic analysis	Exergoeconomic analysis	Exergoenvironmental analysis	SI
η_{TH}	η_{EFF}							
80%	74.6%	1.37%	Energy cost of the DP-STAC 0.077 USD/kWh	DP-STAC can mitigate 39.95 tons of CO_2 over its life cycle (10 years)	Carbon credits earned 579.27 USD	Exergoeconomic parameter 0.1716 kWh/USD	Exergoenvironmental parameter 0.5305 tons of CO_2 over its life cycle (10 years)	1.0138

Table 3 summarizes the results calculated using the analysis equations in Table 1.

Conclusions

The main findings of the present research can be summarized as follows:

- The investigation of a DP-STAC with staggered turbulators demonstrates improved efficiency compared to a traditional smooth plate STAC. At P'_{BF}/P_{BF}= 0.65, B/H_{BF}= 3.5, and P_{BF}/H_{BF}= 1.5, The optimum value of η_{TH},η_{EFF}, and η_{EX} are found to be 80.2%, 74.6%, and 1.37%, respectively.
- According to economic analysis, the energy cost of DP-STAC is 0.077 USD/kWh, while the exergoeconomic and exergoenvironmental parameters are 0.1716

kWh USD^{-1} and 0.5305 tons of CO_2 over its life cycle, respectively.
- The energy payback time is 0.31 years, whereas the exergy payback time is significantly longer at 24.07 years, indicating rapid energy recovery but slow exergy-based returns.
- The system can mitigate 39.95 tons of CO_2 over its life cycle, earning approximately 579.27 USD carbon credits, highlighting its sustainability potential in decreasing greenhouse gas emissions.

Limitations and challenges

- The MATLAB simulation of the analytical model gives a systematic evaluation of the system performance; however, in the case of highly fluctuating outdoor conditions, minor deviations can occur from the actual results.
- Steady-state condition assumption gives a clear interpretation of the thermodynamic behavior of the system, but in actual weather conditions, a transient short-term variation can occur during experimentation.
- The staggered turbulators create turbulence in the main fluid flow and hence enhance the HT rate. This increase in heat transfer is due to the increased pressure drop, which requires more pumping power. The practical design requires a compromise between the HT rate and the pumping power requirement.
- Economic, environmental, and SI are calculated with earlier established formulations; other alternative approaches may offer additional perspectives on the system evaluation.

Supplementary Information The online version contains supplementary material available at https://doi.org/10.1007/s10973-026-15833-5.

Aknowledgments The authors employed generative AI tools, such as DeepSeek by DeepSeek and ChatGPT by OpenAI, to enhance the manuscript's language and readability. Following the use of these tools, the authors thoroughly investigated and revised the text as necessary, and they accept full responsibility for the publication's content.

Author contribution Abhishek Thakur involved in conceptualization, methodology, validation, formal analysis, investigation, resources, data curation, writing—original draft. Sashank Thapa performed conceptualization, methodology, validation, formal analysis, investigation, resources, writing—original draft. Tej Singh contributed to conceptualization, methodology, validation, formal analysis, investigation, visualization, writing—original draft. Raj Kumar performed conceptualization, methodology, validation, formal analysis, investigation, resources, writing—original draft, visualization, supervision. Daeho Lee involved in conceptualization, methodology, validation, formal analysis, investigation, writing—original draft, visualization. Hüseyin Bakır performed conceptualization, methodology, validation, formal analysis, investigation, writing—original draft. Ümit Ağbulut contributed to conceptualization, methodology, validation, formal analysis, investigation, writing—original draft.

Funding Open access funding provided by the Scientific and Technological Research Council of Türkiye (TÜBİTAK). This work was supported by the National Research Foundation of Korea (NRF) grant funded by the Korea Government (MSIT) (RS-2024–00352425), and by the Gachon University Research Fund of 2025 (GCU2025-03230001).

Data availability Data are available from the authors at reasonable request.

Declarations

Conflict of interest The authors declare that they have no known competing financial interests or personal relationships that could have appeared to influence the work reported in this paper.

Open Access This article is licensed under a Creative Commons Attribution 4.0 International License, which permits use, sharing, adaptation, distribution and reproduction in any medium or format, as long as you give appropriate credit to the original author(s) and the source, provide a link to the Creative Commons licence, and indicate if changes were made. The images or other third party material in this article are included in the article's Creative Commons licence, unless indicated otherwise in a credit line to the material. If material is not included in the article's Creative Commons licence and your intended use is not permitted by statutory regulation or exceeds the permitted use, you will need to obtain permission directly from the copyright holder. To view a copy of this licence, visit http://creativecommons.org/licenses/by/4.0/.

References

1. Yadav AK, Kumar R, Wang M, Fekete G, Singh T. Comparative analysis of daily global solar radiation prediction using deep learning models inputted with stochastics variables. Sci Rep. 2025;15:10786.
2. Chen Y, Sha A, Lu Q, Jiang W, Cao Y, Hu K. Solar-to-heat conversion control of pavement through thermochromic coating: Integration of thermal management and visual temperature indication. Energy. 2025;333:137383.
3. Amara WB, Bouabidi A, Chrigui M. Experimental studies and 3D simulations for the investigation of thermal performances of a solar air heater with different spiral-shaped baffles heights. J Build Eng. 2023;65:105662.
4. Abdelkader TK, Fan Q, Gaballah ES, Wang S, Zhang Y. Energy and exergy analysis of a flat-plate solar air heater artificially roughened and coated with a novel solar selective coating. Energies. 2020;13(4):997.
5. Rajendra K. Thermo-hydraulic performance of solar air heater with finned absorber plate forming multiple rectangular air flow passages in parallel under laminar flow conditions. Appl Therm Eng. 2023;221:119673.
6. Abed QA, Badescu V, Ciocanea A, Soriga L, Bureţea D. Models for new corrugated and porous solar air collectors under transient operation. J Non-Equilib Thermodyn. 2017;42(1):79–97.
7. Thapa S, Kumar R, Lee D. Energetic and exergetic analysis of jet impingement solar thermal collector featuring discrete multi-arc shaped ribs absorber surface. Energy. 2024;306:132392.
8. Arunkumar HS, Karanth KV, Kumar S. Review on the design modifications of a solar air heater for improvement in the thermal performance. Sustain Energy Technol Assess. 2020;39:100685.

9. Ravi RK, Saini RP. A review on different techniques used for performance enhancement of double pass solar air heaters. Renew Sustain Energy Rev. 2016;56:941–52.
10. Pachori H, Baredar P, Sheorey T, Gupta B, Verma V, Hanamura K, et al. Sustainable approaches for performance enhancement of the double pass solar air heater equipped with energy storage system: A comprehensive review. J Energy Storage. 2023;65:107358.
11. El-khawajah MF, Aldabbagh LBY, Egelioglu F. The effect of using transverse fins on a double pass flow solar air heater using wire mesh as an absorber. Sol Energy. 2011;85:1479–87.
12. Abo-Elfadla S, Hassana H, El-Dosokya MF. Study of the performance of double pass solar air heater of a new designed absorber: An experimental work. Sol Energy. 2020;198:479–89.
13. Baig W, Ali HM. An experimental investigation of performance of a double pass solar air heater with foam aluminum thermal storage medium. Case Stud Therm Eng. 2019;14:100440.
14. Sajawal M, Rehman T, Ali HM, Sajjad U, Raza A, Bhatti MS. Experimental thermal performance analysis of finned tube-phase change material based double pass solar air heater. Case Stud Therm Eng. 2019;15:100543.
15. Omojaro AP, Aldabbagh LBY. Experimental performance of single and double pass solar air heater with fins and steel wire mesh as absorber. Appl Energy. 2010;87:3759–65.
16. Aldabbagh LBY, Egelioglu F, Ilkan M. Single and double pass solar air heaters with wire mesh as packing bed. Energy. 2010;35:3783–7.
17. El-Sebaii AA, Aboul-Enein S, Ramadan MRI, Shalaby SM, Moharram BM. Investigation of thermal performance of-double pass-flat and v-corrugated plate solar air heaters. Energy. 2011;36:1076–86.
18. Raj AK, Kunal G, Srinivas M, Jayaraj S. Performance analysis of a double-pass solar air heater system with asymmetric channel flow passages. J Therm Anal Calorim. 2019;136:21–38.
19. Kumar PG, Sakthivadivel D, Balaji K, Salman M, Kim SC. Performance enhancement of a double pass solar air heater with a shot-blasted absorber plate and winglets. J Mech Sci Technol. 2021;35(6):2743–53.
20. Thakur A, Kumar R, Lee D, Kumar S, Kumar P, Asif M, et al. Improved performance evaluation of a dual passage solar thermal collector using staggered turbulators. Therm Sci Eng Prog. 2024;53:102668.
21. Assadeg J, Al-Waeli AHA, Fudholi A, Sopian K. Energetic and exergetic analysis of a new double pass solar air collector with fins and phase change material. Sol Energy. 2021;226:260–71.
22. Hedayatizadeh M, Sarhaddi F, Safavinejad A, Ranjbar F, Chaji H. Exergy loss-based efficiency optimization of a double-pass/glazed v-corrugated plate solar air heater. Energy. 2016;94:799–810.
23. Abo-Elfadl S, Yousef MS, Hassan H. Energy, exergy, and enviroeconomic assessment of double and single pass solar air heaters having a new design absorber. Process Saf Environ Prot. 2021;149:451–64.
24. Fahmi MS, Khalil WH, Shareef AJ. Energy and exergy analysis of a finned-plate double pass solar air heater with different arrangement. J Power Energy Eng. 2020;8:1–17.
25. Velmurugan P, Kalaivanan R. Energy and exergy analysis in double-pass solar air heater. Sadhana. 2016;41(3):69–376.
26. Machi MH, Al-Neama MA, Buzás J, Farkas I. Energy-based performance analysis of a double pass solar air collector integrated to triangular shaped fins. Int J Energy Environ Eng. 2022;13:219–29.
27. Dittus FW, Boelter LMK. Heat transfer in automobile radiators of the tubular type. Int Commun Heat Mass Transf. 1985;12:3–22.
28. Bhatti MS. Turbulent and transition flow convective heat transfer in ducts. Handbook of single-phase convective heat transfer 1987. Wiley, New York.
29. Alrashidi A, Altohamy AA, Abdelrahman MA, Elsemary IM. Energy and exergy experimental analysis for innovative finned plate solar air heater. Case Stud Therm Eng. 2024;59:104570.
30. Pachori H, Choudhary T, Sheorey T, Shukla AK, Verma V. A novel energy, exergy and sustainability analysis of a decentralized solar air heater integrated with V-shaped artificial roughness for solar thermal application. Sustain Energy Technol Assess. 2024;66:103816.
31. Duffie JA, Beckman WA. Solar engineering of thermal processes. 3rd ed. Wiley, New York: Wiley Inter science publications; 1980.
32. Biondi P, Cicala L, Farina G. Performance analysis of the solar air heater of Conventional design. Sol Energy. 1988;41(1):101–7.
33. Cortes A, Piacentini R. Improvement of the efficiency of a bare solar collector by means of turbulence promoters. Appl Energy. 1990;36:253–61.
34. Singh VP, Jain S, Karn A, Kumar A, Dwivedi G, Meena CS, et al. Mathematical modeling of efficiency evaluation of double-pass parallel flow solar air heater. Sustain. 2022;14:10535.
35. Altfeld K, Leiner W, Fiebig M. Second law optimization of flat-plate solar air heaters, part I: the concept of net exergy flow and the modelling of solar air heaters. Sol Energy. 1988;41(2):127–32.
36. Kumar A, Kumar R, Bhushan A. Differential exergy investigation and environ-economic assessment of a dimpled plate and flat plate solar air heater under turbulent conditions. Appl Therm Eng. 2024;240:122299.
37. Abo-Elfadl S, Yousef MS, El-Dosoky MF, Hassan H. Energy, exergy, and economic analysis of tubular solar air heater with porous material: an experimental study. Appl Therm Eng. 2021;196:117294.
38. Hassan H, Yousef MS, Abo-Elfadl S. Energy, exergy, economic and environmental assessment of double pass V-corrugated-perforated finned solar air heater at different air mass ratios. Sustain Energy Technol Assess. 2021;43:100936.
39. Fattoum R, Hidouri A, Attia MEH, Arici M, Abbadsi MA. Optimization of solar air heaters performance using parallel porous wire mesh: energy, exergy, and enviro-economic analysis. Therm Sci and Eng Prog. 2024;48:102385.
40. Elbar ARA, Yousef MS, Hassan H. Energy, exergy, exergoeconomic and enviroeconomic (4E) evaluation of a new integration of solar still with photovoltaic panel. J Clean Prod. 2019;233:655–80.
41. Kumar D, Mahanta P, Kalita P. Performance analysis of a solar air heater modified with zig-zag shaped copper tubes using energy-exergy methodology. Sustain Energy Technol Assess. 2021;46:101222.
42. Albdoor AK, Obaid ZAH, Kamel MS, Azzawi IDJ. Energy, exergy, economic and environmental analysis of a solar air heater integrated with double triangular fins: Experimental investigation. Int J Thermofluids. 2024;24:100979.
43. Goswami DY, Kreith F, Kreider JF. Principles of solar engineering. 2nd ed. New York: Taylor & Francis Group; 2000.
44. Kreith F, Berger SA. Mechanical engineering handbook. CRC Press; 1999. Boca Raton, ch.3.
45. Agrawal Y, Bhagoria JL, Gautam A, Chaurasiya PK, Dhanraj JA, Solomon JM, et al. Experimental evaluation of hydrothermal performance of solar air heater with discrete roughened plate. Appl Therm Eng. 2022;211:118379. https://doi.org/10.1016/j.applthermaleng.2022.118379.

Publisher's Note Springer Nature remains neutral with regard to jurisdictional claims in published maps and institutional affiliations.